

Decoupling of temporal/spatial broadening effects in Doppler wind LiDAR by 2D spectral analysis

Zhen Liu(刘珍), Yun-Peng Zhang(张云鹏), Xiao-Peng Zhu(竹孝鹏), Ji-Qiao Liu(刘继桥), De-Cang Bi(毕德仓), and Wei-Biao Chen(陈卫标)

Citation: Chin. Phys. B, 2024, 33 (**3**): 034214. DOI: 10.1088/1674-1056/ad10fd
Journal homepage: http://cpb.iphy.ac.cn; http://iopscience.iop.org/cpb

What follows is a list of articles you may be interested in

Raman lasing and other nonlinear effects based on ultrahigh-*Q* CaF_2 optical resonator

Tong Xing(邢彤), Enbo Xing(邢恩博), Tao Jia(贾涛), Jianglong Li(李江龙), Jiamin Rong(戎佳敏), Yanru Zhou(周彦汝), Wenyao Liu(刘文耀), Jun Tang(唐军), and Jun Liu(刘俊)

Chin. Phys. B, 2022, 31 (**10**): 104204. DOI: 10.1088/1674-1056/ac8728

Research of NO_2 vertical profiles with look-up table method based on MAX-DOAS

Yingying Guo(郭映映), Suwen Li(李素文), Fusheng Mou(牟福生), Hexiang Qi(齐贺香), and Qijin Zhang(张琦锦)

Chin. Phys. B, 2022, 31 (**1**): 014212. DOI: 10.1088/1674-1056/ac1415

A scanning distortion correction method based on *X*- *Y* galvanometer Lidar system

Bao-Ling Qi(漆保凌), Chun-Hui Wang(王春晖), Dong-Bing Guo(郭东兵), and Bin Zhang(张斌)

Chin. Phys. B, 2021, 30 (**4**): 044206. DOI: 10.1088/1674-1056/abcf42

Multi-wavelength continuous-wave Nd:YVO_4 self-Raman laser under in-band pumping

Li Fan(樊莉), Xiao-Dong Zhao(赵孝冬), Yun-Chuan Zhang(张蕴川), Xiao-Dong Gu(顾晓东), Hao-Peng Wan(万浩鹏), Hui-Bo Fan(范会博), Jun Zhu(朱骏)

Chin. Phys. B, 2019, 28 (**8**): 084210. DOI: 10.1088/1674-1056/28/8/084210

Structural, vibrational, optical, photoluminescence, thermal, dielectric, and mechanical studies on zinc (tris) thiourea sulfate single crystal: A noticeable effect of organic dye

Mohd Shkir, V Ganesh, S AlFaify, I S Yahia, Mohd Anis

Chin. Phys. B, 2018, 27 (**5**): 054216. DOI: 10.1088/1674-1056/27/5/054216

Decoupling of temporal/spatial broadening effects in Doppler wind LiDAR by 2D spectral analysis

Zhen Liu(刘珍)[1,2], Yun-Peng Zhang(张云鹏)[1,†], Xiao-Peng Zhu(竹孝鹏)[1], Ji-Qiao Liu(刘继桥)[1], De-Cang Bi(毕德仓)[1,2], and Wei-Biao Chen(陈卫标)[1,2,‡]

[1] *Space Laser Engineering Department, Shanghai Institute of Optics and Fine Mechanics, Chinese Academy of Sciences, Shanghai* 201800, *China*

[2] *Center of Materials Science and Optoelectronics Engineering, University of Chinese Academy of Sciences, Beijing* 100049, *China*

(Received 20 October 2023; revised manuscript received 21 November 2023; accepted manuscript online 30 November 2023)

Pulse echo accumulation is commonly employed in coherent Doppler wind LiDAR (light detection and ranging) under the assumption of steady wind. Here, the measured spectral data are analyzed in the time dimension and frequency dimension to cope with the temporal wind shear and achieve the optimal accumulation time. A hardware-efficient algorithm combining the interpolation and cross-correlation is used to enhance the wind retrieval accuracy by reducing the frequency sampling interval and then reduce the spectral width calculation error. Moreover, the temporal broadening effect and spatial broadening effect are decoupled according to the strategy we developed.

Keywords: Doppler wind LiDAR, spectral analysis, hardware efficiency, spectrum broadening effects

PACS: 42.68.Wt, 42.79.Qx **DOI:** 10.1088/1674-1056/ad10fd

1. Introduction

Wind data is important in fields such as environmental monitoring,[1] aviation safety,[2,3] wind energy site selection,[4] and weather forecasting.[1,5] For example, the numerical meteorological model is composed of fundamental components, such as wind, humidity, temperature, and pressure, where high-accuracy wind information within the lower atmosphere is one of the most important parameters.[6,7] LiDAR (light detection and ranging), a widely used optical remote sensing tool, plays an increasingly important role.[8–12] Coherent detection and direct detection are two schemes used in Doppler LiDAR to obtain wind information.[13] The main difference between these two methods lies in the extraction of Doppler frequency shifts. Compared with direct detection,[14] coherent detection has the advantages of a high signal-to-noise ratio, high detection sensitivity, insensitivity to background sunlight, and superior measurement accuracy.[15–17]

To improve the accuracy of wind retrieval, it is necessary to perform an incoherent accumulation of echo pulses.[18] It is commonly assumed that the wind speed remains constant in this process.[18–20] In fact, wind speed may vary with time domain or space domain, leading the spectrum to broaden.[21] Therefore, the constant-wind assumption is not valid in certain situations, particularly in the presence of wind shear. Low-level wind shear, which is characterized by sudden temporal shift, spatial shift, and high intensity, is a hazardous meteorological phenomenon.[21,22] Global statistics from 1980 to 1996 recorded 621 significant aviation accidents, 46% of which occurred during landings. Wind shear is a major cause of severe accidents. The main reason for this is the lack of highly accurate wind data. Therefore, it is imperative to consider the influence of wind shear on wind retrieval.

To address this issue, we propose a two-dimensional (2D) spectral analysis method that partially relaxes the constant-wind assumption and determines the optimal accumulation time for wind retrieval. Meanwhile, a field-programmable gate array (FPGA)-compatible algorithm called interpolated cross-correlation (ICC) is employed in the processing of backscattered spectra, which improves the wind retrieval performance. By providing a finer digital spectrum shape, this method results in better spectrum moment accuracy and an extended detection range. Furthermore, we develop a strategy to decouple the temporal broadening effect and spatial broadening effect of the spectrum based on the relationship between the spectral width and accumulation time, facilitating an understanding of the causes of spectrum broadening.

The rest of this paper is organized as follows. In Section 2, the principle of coherent Doppler wind LiDAR and the interpolated cross-correlation method are reviewed. In Section 3, the optimal accumulation time of pulse echo signal is discussed and the strategy that can decouple the temporal broadening effect and spatial broadening effect is presented. Finally, in Section 4, the conclusions are drawn from the present study.

[†]Corresponding author. E-mail: zhangyunpeng@siom.ac.cn
[‡]Corresponding author. E-mail: wbchen@siom.ac.cn

© 2024 Chinese Physical Society and IOP Publishing Ltd

2. Principle of coherent Doppler wind LiDAR and interpolated cross-correlation method

Figure 1 shows a schematic of the experimental setup for the coherent Doppler wind LiDAR, which is composed of a laser, transmit and receive optical path, telescope, heterodyne detection unit, data acquisition unit, and processing unit.[17] The single-frequency laser is operated at a central wavelength of 1540 nm. It is split into local oscillator (LO) and seed light by using a beam splitter (BS). The seed light is chopped and frequency-shifted by 160 MHz by using an acousto–optic modulator (AOM) to produce pulsed light with a pulse width of 400 ns and a repetition frequency of 5 kHz. After being amplified by using an erbium-doped fiber amplifier (EDFA), the laser pulses are transmitted to the circulator and emitted into the atmosphere through a telescope with an aperture of about 100 mm. Because the system employs a coaxial transceiver, the telescope also acts as a collector and receives backscattered signals from atmospheric aerosols. The received signal is combined with LO light by using a 2×2 mixer and detected by using a balanced detector (BD) with a bandwidth of 350 MHz. Finally, the received signal is processed by using an analog-to-digital converter (ADC), FPGA, and personal computer (PC).

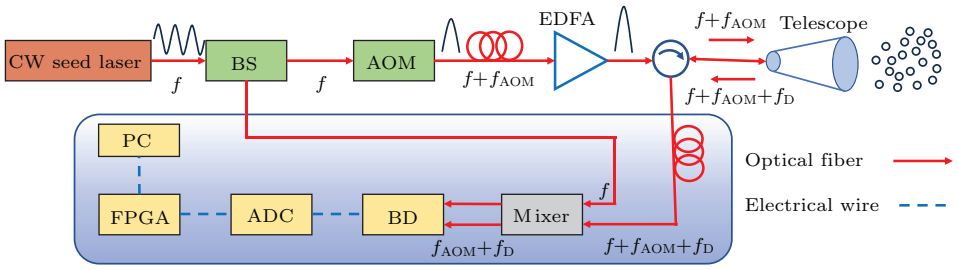


Fig. 1. Schematic diagram of coherent Doppler wind LiDAR experimental setup.

In practical applications, to ensure the calculation speed of the hardware, the fast Fourier transform (FFT) point number in the FPGA is typically set to 512 or 1024.[23] When the sampling rate is high, the consequent high-frequency sampling interval leads the wind retrieval accuracy to deteriorate. Similarly, if the spectral width is calculated, the corresponding calculation error increases. The zero-padding method can be used to increase the number of fast FFT points.[24,25] Although it can effectively improve the sampling frequency of the spectrum, a significant computational load is introduced, which affects the real-time measurement capability. Data fitting[26] and cross-correlation.[27–30] are usually used to enhance the peak identification capability of signals interfered by noise. However, nonlinear fitting is often subject to initial value dependency, and the iterative progress is unfriendly to the FPGA. Thus, we develop a hardware-efficient center frequency retrieval algorithm, which combines the cross-correlation method and interpolation method. Furthermore, by reducing the sampling interval in the frequency domain, the accuracy of the spectral width calculation can be improved, especially in the scenarios with low signal-to-noise ratio or narrow spectral width. Then, we use the FFT properties for interpolation after cross-correlation. This method utilizes high hardware efficiency.

The cross-correlation in the frequency domain is equivalent to multiplication in the time domain, and interpolation can be realized with zero padding during the FFT.[31] Therefore, the ICC algorithm inherits the hardware efficiency of the FFT algorithm. The reference spectrum used in the cross-correlation is derived from a pulsed laser. We perform an FFT on a Gaussian pulse to obtain the corresponding reference spectrum. Because a Gaussian pulse is a real symmetrical signal, the reference spectrum is also real and symmetrical.

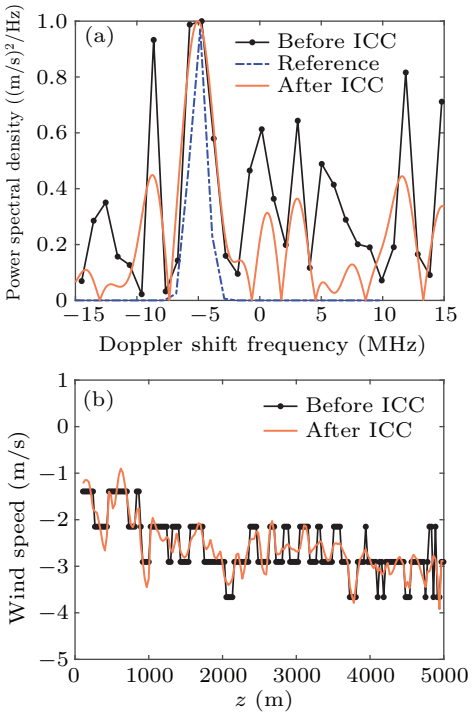


Fig. 2. (a) Backscattered spectrum at 4400 m and (b) wind retrieval results before and after interpolated cross-correlation (ICC).

First, an inverse fast Fourier transform (IFFT) is performed on the backscattered and reference spectra to obtain their equivalent time-domain signals (ETS). The ETS of the cross-correlation of spectrum is obtained by multiplying the

two equivalent time domain signals, namely, the backscattering spectrum and reference spectrum. Finally, the cross-correlation spectrum is obtained from the magnitude of the Fourier-transformed ETS, and zero padding is performed in the last FFT process to realize interpolation. The entire process can be expressed by

$$\mathrm{ETS}_{x\mathrm{corr}} = \mathrm{IFFT}\left[\mathrm{PSD}_{\mathrm{m}}\right] \cdot \mathrm{IFFT}\left[\mathrm{PSD}_{\mathrm{ref}}\right], \tag{1}$$

$$\mathrm{PSD}_{x\mathrm{corr}} = \left|\mathrm{FFT}\left[\mathrm{ETS}_{x\mathrm{corr}}\right]\right|, \tag{2}$$

where PSD stands for the power spectral density and the subscripts m, ref, and *x*corr refer to the measured signal, reference signal, and their cross-correlation, respectively. The advantage of this method in computational complexity is that only one zero padding is needed on the cumulative spectrum instead of the echo of each pulse.

To better illustrate the effectiveness of this approach, the backscattered spectra before and after ICC at a detection distance of 4400 m are shown in Fig. 2(a) as an example. The frequency sampling intervals before and after ICC are 0.98 MHz and 0.03 MHz, respectively. It is evident that the signal peak becomes more prominent and the spectrum becomes smoother after ICC, which can be beneficial to Doppler frequency shift and spectral width retrieval. Figure 2(b) presents the wind retrieval results before and after ICC, demonstrating that a finer wind-field structure can be obtained after ICC. In addition, some wind retrieval fluctuations occur about 4800 m before the ICC, whereas they do not occur after the ICC. This indicates that the ICC method can improve detection performance to a certain extent.

3. Results and discussion

The accumulation time can be optimized by using the ICC algorithm. Considering the potential temporal or spatial variability of the wind field, pulse accumulation time should be as short as possible. However, if the pulse accumulation number is too small, the signal is seriously disturbed by noise.[32] Therefore, it is necessary to balance the pulse accumulation number with the influence of the noise. In order to achieve this balance, the minimum pulse accumulation number is set as the basic processing unit. The optimal pulse accumulation time is then determined by comparing the PSD of the backscattered spectra[33] with different pulse accumulation numbers.

Specifically, the wind speed at the same detection distance is retrieved by block averaging when the values of pulse accumulation number N are 50, 100, 125, and 200 as shown in Fig. 3. It can be seen from Figs. 3(a) and 3(b) that the wind retrieval results are inaccurate when N is small. In contrast, when $N = 125$, the wind retrieval results are between -3.7 m/s and -2.9 m/s, which is relatively reasonable as shown in Fig. 3(c). When $N = 200$, the wind retrieval results are similar to those for $N = 125$ as shown in Fig. 3(d). Therefore, we set the minimum pulse accumulation number to 125 for the subsequent analysis.

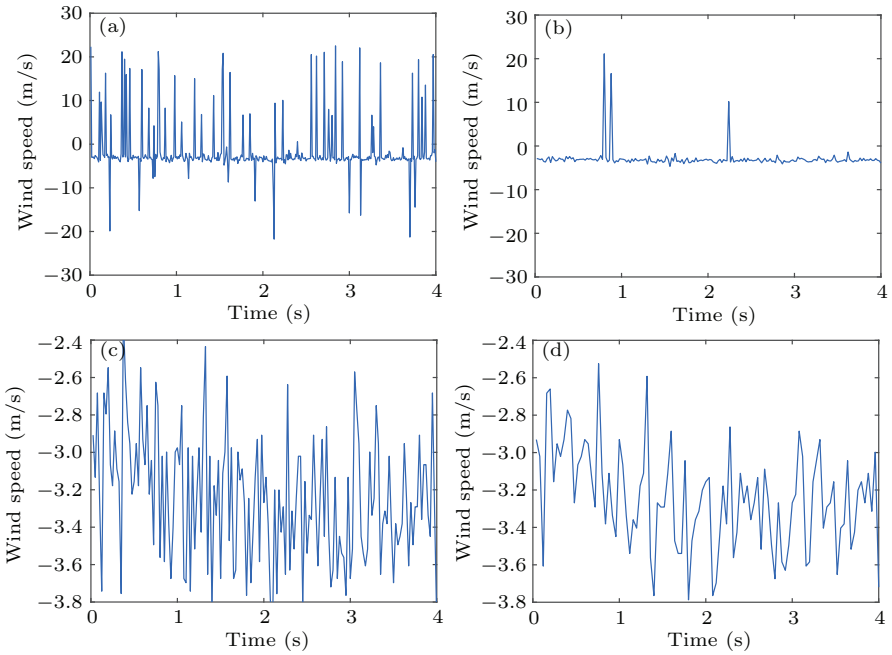


Fig. 3. Wind retrieval results at the same detection distance with accumulation number $N = 50$ (a), 100 (b), 125 (c), and 200 (d).

Figure 4 shows the PSDs of wind speed within the 5000-m range, corresponding to accumulation time of 0.1 s, 0.25 s, and 0.5 s, respectively. From Fig. 4 it can follow that the optimal accumulation time can be determined for a given range and atmosphere condition. The variability in wind data is attributed to wind turbulence, which follows Kolmogorov's law, and its PSD is directly proportional to $f^{-5/3}$.[34] The log–log plot of the PSD shows that the fitted wind turbulence slope

of -1.8 matches the Kolmogorov turbulence slope of $-5/3$ closely as shown by the solid red lines and dashed purple lines in Fig. 4. The root mean square (RMS) of the wind speed measurement error is estimated by integrating the noise at the lower end of the spectrum. Figure 4(a) shows that the frequency at which the PSD begins to flatten (*i.e.*, the frequency cutoff) is 3.54 Hz, corresponding to an RMS value of 0.234 m/s. In other words, when the accumulation time is less than 0.28 s, the accuracy of the wind speed measurement cannot be improved any more. The accumulation time shown in Fig. 4(b) is close to the optimal accumulation time, which minimizes the redundancy and loss of wind information. Conversely, the accumulation time in Fig. 4(c) is too long, resulting in a noticeable loss of wind data. Therefore, the pulse accumulation time of 0.25 s will be adopted. It is important to note that the specific scenarios may require case-by-case analysis to determine the optimal accumulation time based on measured wind data.

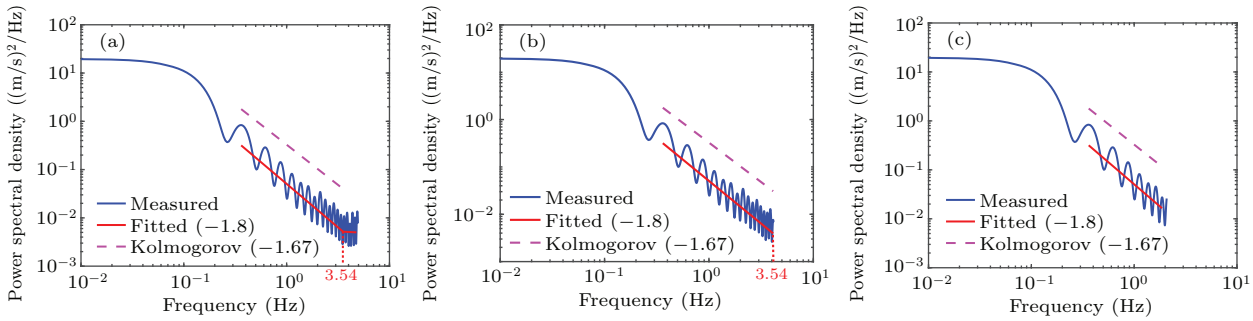


Fig. 4. Wind PSD at different accumulation time 0.1 s (a), 0.25 s (b), 0.5 s (c).

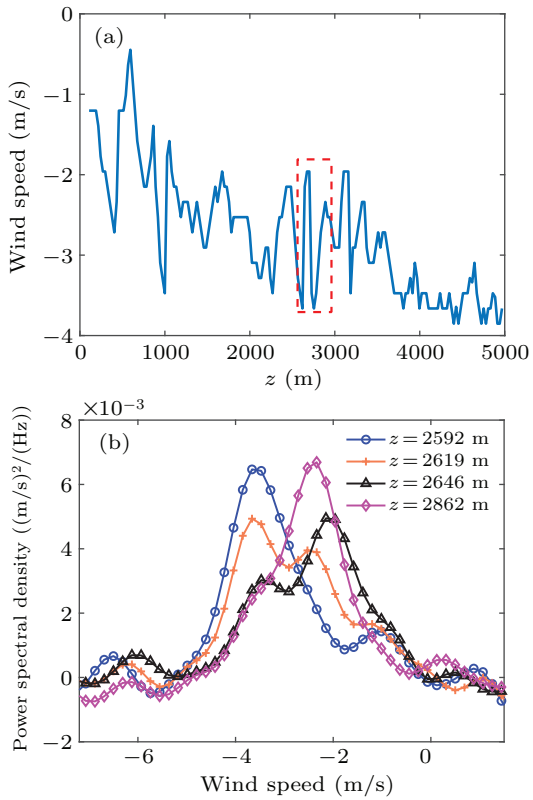


Fig. 5. (a) Radial wind speed varying with distance and (b) backscattered spectra in wind shear region.

Figure 5(a) displays the wind speed measured at a specific time, where the locations with rapid wind speed changes indicate the phenomenon of wind shear as reflected by large gradients in the wind speed profile. As an example, the backscattered spectra corresponding to the wind data in the red dotted box of Fig. 5(a) are shown in Fig. 5(b). It is obvious that the position of the spectral peak is shifted and the spectrum is broadened within 270 m, which indicates the existence of wind shear.[35]

In order to effectively identify and explore the cause of wind shear, we propose a decoupling strategy for temporal/spatial broadening effects[35,36] to better understand the wind shear. As shown in Fig. 6, this strategy relies mainly on the analysis of the value and trend of the spectral width. The spectral width is evaluated at different accumulation times, and the broadening effects are classified through two criteria, focusing on the minimum value and the trend of the spectral width. The minimum width criterion is related to the spatial broadening effect, and the trend criterion is dependent on temporal broadening effect. The two criteria can be explained as follows.

Figure 7 shows four typical evolution patterns of the spectral widths. The blue curve shows that the spectral width first decreases and then stabilizes with an increase with accumulation time increasing, and the minimum spectral width is close to an ideal spectral width, indicating that neither temporal broadening effect nor spatial broadening effect exists at this position. The orange curve shows that the spectral width first decreases and then increases with accumulation time increasing, which reveals that the spectral peak at this position moves with time. As the accumulation time increases, the spectrum broadens, indicating a temporal broadening effect. The performance trend of the black curve is the same as that of the blue curve, except that the minimum spectral width exceeds the ideal spectral width. In addition, the accumulation time corresponding to flattening is shorter, indicating that there are

multiple changes in the wind speed within a distance gate, implying spatial broadening effects. The purple curve indicates both temporal broadening effect and spatial broadening effect at this location. Notably, for all four curves, the spectral width decreases with the increase of accumulation time within 0.1 s. The main reason for this is that the signal is more seriously affected by noise when the accumulation time is too short; therefore, the estimation of spectral width is inaccurate.

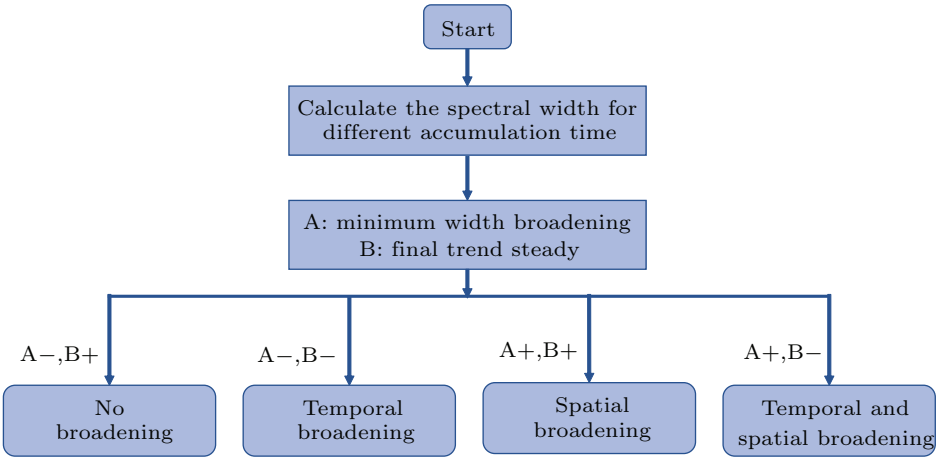


Fig. 6. Flowchart of decoupling of temporal broadening effect and spatial broadening effect.

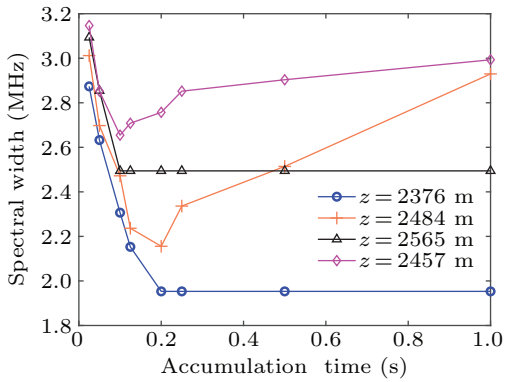


Fig. 7. Spectral widths varying with accumulation time.

4. Conclusions

In this work, we analyzed the signal spectrum of a coherent Doppler LiDAR and introduced a 2D spectral analysis method to enhance the retrieval capability of Doppler signals. An ICC method is proposed to improve the retrieval precision of the Doppler frequency and spectral width with low computational load. By relaxing the assumption of wind field stability during multi-pulse accumulation, we developed a strategy to obtain an optimal accumulation time and decouple the temporal broadening effect, and spatial broadening effect of the wind shear. The proposed method is validated experimentally, and can have further implications in areas like aviation safety.

Acknowledgement

Project supported by the Shanghai Science and Technology Innovation Action (Grant No. 22dz1208700).

References

[1] Yang Y J, Yim S H L, Haywood J, Osborne M, Chan J C S, Zeng Z L and Cheng J C H 2019 *J. Geophys. Res.* **124** 16
[2] Wu S H, Zhao X C and Liu B Y 2019 *Opt. Express* **27** 1142
[3] Li J, Shen C, Gao H, Chan P W, Hon K K and Wang X 2020 *Opt. Express* **28** 4286
[4] Larsen T J, Madsen H A, Larsen G C and Hansen K S 2013 *Wind. Energy* **16** 605
[5] Tsai Y S, Miau J J, Yu C M and Chang W T 2019 *Boundary Layer Meteorol.* **171** 237
[6] Asaka K, Yanagisawa T and Hirano Y 2001 *Proceedings of the Lidar Remote Sensing for Industry and Environment Monitoring*, October 9–12, Sendai, Japan p. 321
[7] Lin Y Q, Zhao Y Q and Ye M 2021 *Opto-Electronic Engineering* **48** 210080
[8] Shangguan M J, Xia H Y, Dou X K, Wang C, Qiu J W, Zhang Y P, Shu Z F and Xue X H 2015 *Chin. Phys. B* **24** 094212
[9] Choukulkar A, Brewer W A, Sandberg S P, Weickmann A, Bonin T A, Hardesty R M, Lundquist J K, Delgado R, Iungo G V, Ashton R, Debnath M, Bianco L, Wilczak J M, Oncley S and Wolfe D 2017 *Atmos. Meas. Tech.* **10** 247
[10] Khachaturian A, Fatemi R and Hajimiri A 2022 *Photon. Res.* **10** A66
[11] Gao F, Gao F J, Yang X, Li G P, Yang F, Li S C, Wang L, Hua D X and Stanič S 2023 *Chin. Opt. Lett.* **21** 030101
[12] Marinov E, Martins R J, Ben Youssef M A, Kyrou C, Coulon P M and Genevet P 2023 *Adv. Photon.* **5** 046005
[13] Zhang F F, Dou X K, Sun D S, Shu Z F, Xia H Y, Gao Y Y, Hu D D and Shangguan M J 2014 *Opt. Eng.* **53** 124102
[14] Zhao R C, Xia H Y, Dou X K, Sun D S, Han Y L, Shangguan M J, Guo J and Shu Z F 2015 *Chin. Phys. B* **24** 024128
[15] Baker W E, Emmitt G D, Robertson F, Atlas R M, Monlinari J E, Bowdle D A and Mcelroy J 1995 *Bull. Am. Meteorol. Soc.* **76** 869
[16] Liu Z L, Barlow J F, Chan P W, Fung J C H, Li Y G, Ren C, Mak H W L and Ng E 2019 *Remote Sens.* **11** 2522
[17] Liu H, Yuan L C, Fan C C, Liu F F, Zhang X, Zhu X P, Liu J Q, Zhu X L and Chen W B 2020 *Opt. Eng.* **59** 014109
[18] Banakh V A, Krivolutskii N P, Smalikho I N and Werner C 2002 *Proceedings of the 9th Joint International Symposium on Atmospheric and Ocean Optics/Atmospheric Physics*, July 2–5, Tomsk, Russia, p. 96
[19] Han F, Han Y L, Sun D S, Hu M Y, Liu H J, Zhou A R, Zhang N N, Jiang S, Chu J Q, Zheng J and Lan J X 2020 *Appl. Opt.* **59** 1037
[20] Khattak A, Chan P W, Chen F and Peng H 2023 *Risk Anal.* **10** 14215

[21] Li L Q, Shao A M, Zhang K J, Ding N and Chan P W 2020 *J. Meteorol. Res.* **34** 633
[22] Michel D T, Dolfi-Bouteyre A, Goular D, Augère B, Planchat C, Fleury D, Lombard L, Valla M and Besson C 2020 *Opt. Express* **28** 14374
[23] Zhao P E, Luo X, Cao W Y, Zhao B, Feng L T, Li X F, Tan J and Zhou D F 2014 *Infrared Laser Eng.* **43** 98
[24] Zhou Y S, Ma X P, Zhao Y M and Li L H 2018 *Infrared Laser Eng.* **47** 306002
[25] Zhang Y P, Wu Y B and Xia H Y 2021 *Opt. Lett.* **46** 5550
[26] Rui X B, Guo P, Chen H, Chen S Y and Zhang Y C 2019 *Opt. Express* **27** 21319
[27] Frehlich R G and Yadlowsky M J 1995 *J. Atmos. Ocean Tech.* **12** 1217
[28] Smalikho I N, Banakh V A, Holzäpfel F and Rahm S 2015 *Opt. Express* **23** A1194
[29] Zaslawski S, Yang Z S and Thevenaz L 2020 *J. Light. Technol.* **38** 3723
[30] Wang G, Pang Z W, Zhang B H, Wang F M, Chen Y F, Dai H F, Wang B and Wang L J 2022 *Photon. Res.* **10** 433
[31] Zhang Y X, Xie Y M, Li X, Zhang X P and Zhou J Y 2021 *IEEE Trans. Signal Process.* **69** 1
[32] Kotake N, Sakamaki H, Imaki M, Miwa Y, Ando T, Yabugaki Y, Enjo M and Kameyama S 2022 *Opt. Express* **30** 20038
[33] Bouteyre A D, Canat G, Lombard L, Valla M, Durecu A and Besson C 2017 *Opt. Eng.* **56** 031217
[34] Tatsumi T 2011 *J. Phys.: Conf. Ser.* **318** 042024
[35] Yuan J L, Xia H Y, Wei T W, Wang L, Yue B and Wu Y B 2020 *Opt. Express* **28** 37406
[36] Kameyama S, Furuta M and Yoshikawa E 2023 *IEEE Trans. Geosci. Remote Sens.* **61** 1